Multifunctional Radar Sensor for Automotive Application

Michael Wollitzer, J. Buechler, J.-F. Luy, *Senior Member, IEEE,* Uwe Siart, E. Schmidhammer, J. Detlefsen, *Member, IEEE,* and M. Esslinger

***Abstract*—A multifunctional radar system for vehicles consisting of two modules with a combined bistatic/monostatic arrangement is presented. One module acts as a transceiver, whereas the other is a receiving circuit. The transmitting part radiates a frequency-modulated signal alternately in two orthogonal polarizations. The receiving parts work with different local oscillator (LO) frequencies and detect both polarizations of the scattered signal simultaneously. From the resulting Doppler spectra and a distance measurement, the velocity, tilt angle, height with respect to ground, and the direction of the movement of a vehicle can be derived. From the polarimetric information, a classification of the road condition is possible. In a first approach, the sensor was built in a conventional waveguide technique. The second step was to realize the millimeter-wave circuits of both modules with monolithic silicon millimeter-wave integrated circuit (SIMMWIC) technology. To achieve a flat arrangement, a leaky-wave antenna is developed and coupled to the SIMMWIC's.**

***Index Terms*— Active antennas, leaky-wave antennas, radar polarimetry, road vehicle radar, radar position measurement, SIMMWIC.**

I. Introduction

IMPORTANT aspects in future automotive concepts are comfort, reduced energy consumption, and particularly, improved safety. To optimize these points, a precise sensing of the vehicle parameters and the environmental conditions is necessary. For example, the velocity of a vehicle, tilt angle, height above ground, and especially, for active distance control and for autonomous driving, the road condition have to be known. Radar sensors in the millimeter-wave range are well suited to carry out these tasks. A comprehensive overview on the present status of automotive radar sensors is given in [1]. However, separate sensors for each purpose are uneconomic. Thus, the merging of such sensor types to one multifunctional sensor system is needed. Therefore, a millimeter-wave radar system was conceived to measure the mentioned quantities and to get information about the road condition.

Silicon millimeter-wave integrated circuit (SIMMWIC) technology is a promising way to meet the low-cost requirement for mass production. The monolithic integration of active devices combined with antenna structures on high-resistivity silicon leads to complete single-chip transmitter or receiver circuits.

Manuscript received October 28, 1997; revised January 29, 1998. This work was supported by the Federal Ministry of Research and Education (BMBF) under Grant 16 SV 417/0.

M. Wollitzer, J. Buechler, and J.-F. Luy are with the Daimler-Benz Research Center, D-89011 Ulm, Germany.

U. Siart, E. Schmidhammer, and J. Detlefsen are with the Laboratories for High-Frequency Technology, Technische Universität, D-8000 Müunchen, Germany.

M. Esslinger is with the Department of Microwave Techniques, Universität of Ulm, 89081 Ulm, Germany.

Publisher Item Identifier S 0018-9480(98)03388-2.

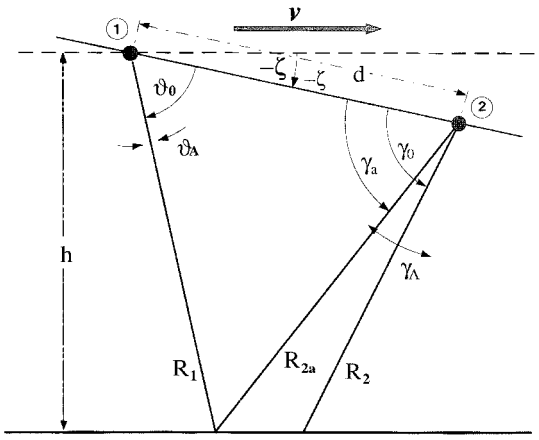

Fig. 1. Sensor arrangement.

II. Sensor Concept

A two-frequency method is used with a combined bistatic/monostatic arrangement of two radar modules, shown in Fig. 1. The radar modules are mounted at a distance d. The angles of the beams with respect to the axis through the modules are ϑ_0 and γ_0, respectively. The beamwidths are ϑ_A and γ_A. The tilt angle of the vehicle is ζ and the height with respect to ground is h. Module 1 is radiating a signal at frequency f_{s1} and, working as a self-mixing oscillator, also receives the back-scattered signal. Module 2, also working as a self-mixing oscillator with nearly zero radiating power at f_{s2} separated by δf from f_{s1}, receives the back-scattered signal. The transmitted signal u_{s1} of module 1 is sinusoidally modulated as follows:

$$u_{s1} = U_{s1}\ \cos[\omega_{s1}t + \eta\sin(\omega_m t - \varphi_m) - \varphi_{s1}] \quad (1a)$$

$$\eta = \frac{\Delta f}{2f_m} \quad (1b)$$

the local oscillator (LO) signal u_{s2} of module 2 is a continuous wave (CW)

$$u_{s2} = U_{s2}\cos[\omega_{s2}t - \varphi_{s2}]. \quad (2)$$

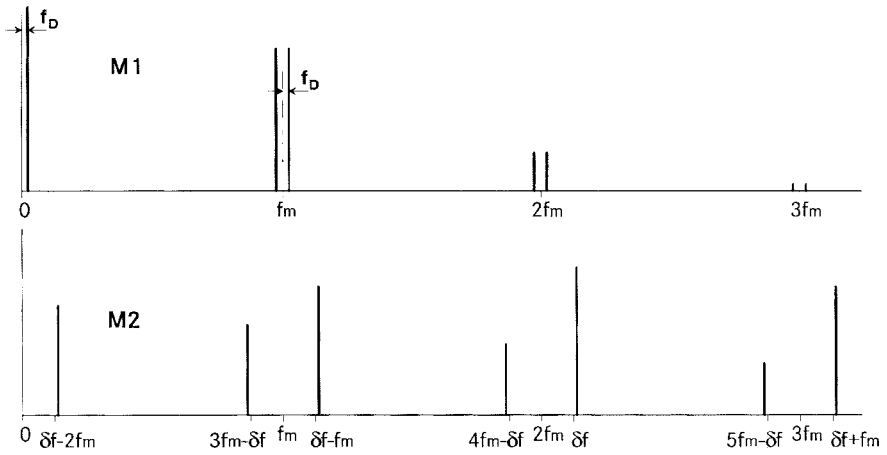

Fig. 2. Spectra of the mixer signals, $df > 2f_m$.

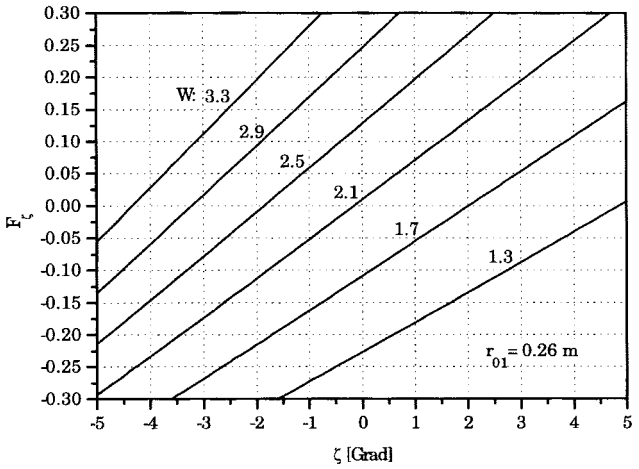

Fig. 3. Function F_ζ for different $W, h = 25$ cm, $d/h = 0.9$.

The time delays of the backscattered signal into module 1 and of the scattered signals into module 2 are

$$\tau_1 = \frac{2R_1(t)}{c} = \frac{2}{c}\left[r_{01} \mp v_{r1}t\right] \tag{3a}$$

$$r_{01} = R_{01} \pm v_{r1}t_0 \tag{3b}$$

$$v_{r1} = v\cos(\vartheta_0 - \zeta) \tag{3c}$$

$$\tau_a = \frac{R_a(t)}{c} = \frac{1}{c}[r_{01} + r_{02a} \mp (v_{r1} - v_{r2a})t] \tag{3d}$$

$$r_{02a} = R_{02a} \pm v_{r2a}t_0 \tag{3e}$$

$$v_{r2a} = v\cos(\gamma_a + \zeta). \tag{3f}$$

Thus, the received signals are

$$u_{e1} = U_{e1}\cos\{\omega_{s1}(t-\tau_1) + \eta\sin[\omega_m(t-\tau_1) - \varphi_m] - \varphi_{s1}\} \tag{4}$$

$$u_{e2} = U_{e2}\cos\{\omega_{s1}(t-\tau_a) + \eta\sin[\omega_m(t-\tau_a) - \varphi_m] - \varphi_{s1}\} \tag{5}$$

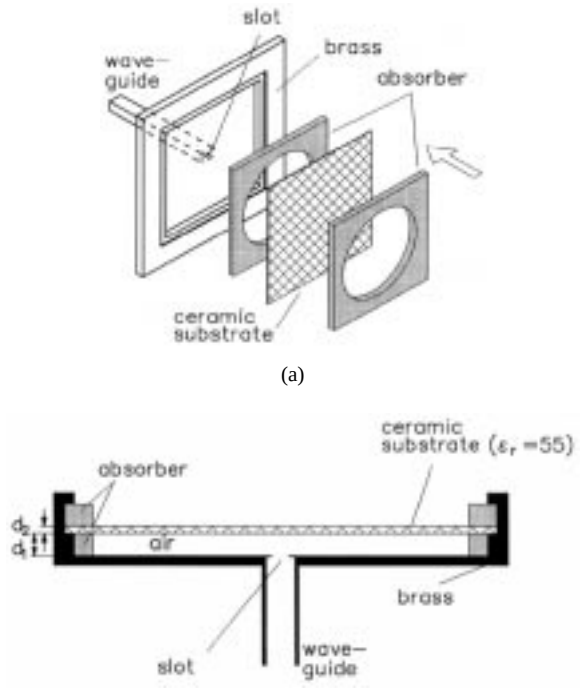

Fig. 4. Principle of leaky-wave antenna.

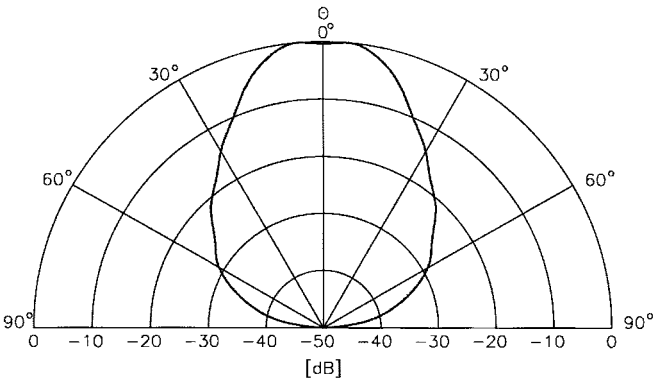

Fig. 5. Calculated radiation pattern of the planar antenna.

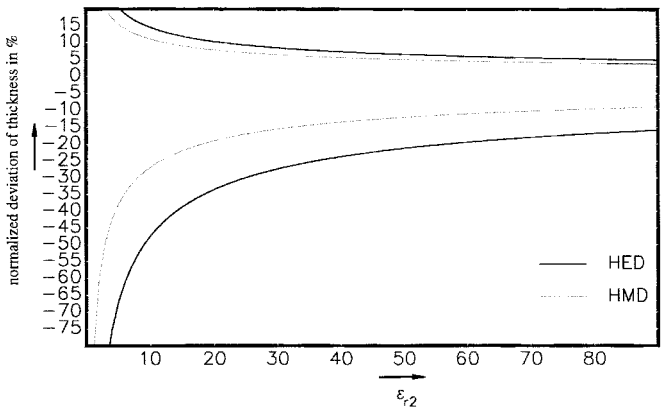

Fig. 6. 3-dB reduction of the antenna gain for varied thicknesses of the dielectric slab.

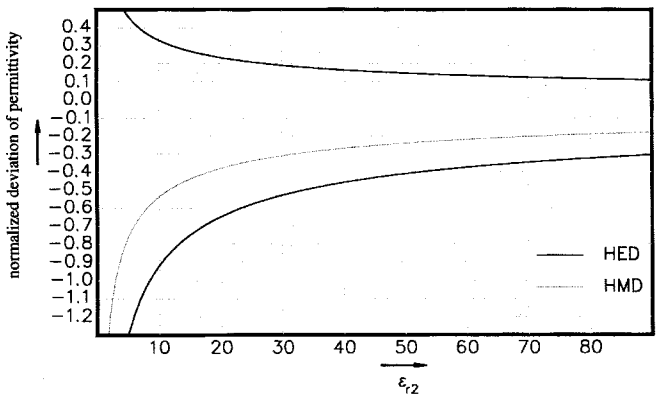

Fig. 7. 3-dB reduction of the antenna gain for varied permittivity of the dielectric slab.

and after down conversion

$$u_{M1}(t) \propto \cos\left[\omega_{s1}\tau_1 + \alpha\cos\left(\omega_m\left(t-\frac{\tau_1}{2}\right)-\varphi_m\right)\right]$$
$$= J_0(\alpha)\cos\Phi_D + 2\sin\Phi_D \sum_{n=0}^{\infty}(-1)^n \cdot J_{2n+1}(\alpha)\cos[(2n+1)x_1] + 2\cos\Phi_D \sum_{n=1}^{\infty}(-1)^n J_{2n}(\alpha)\cos(2nx_1) \quad (6)$$

$$\alpha = \frac{\Delta f}{f_m}\sin\left(\frac{\omega_m\tau_1}{2}\right) \quad (7a)$$

$$x_1 = \left(\omega_m \pm \frac{\omega_{Dm}}{2}\right)t - \frac{\omega_m r_{01}}{c} - \varphi_m \quad (7b)$$

$$\omega_{Dm} = \frac{2\omega_m v_{r1}}{c} \quad (8a)$$

$$\Phi_D = \pm\omega_D t - \frac{2\omega_{s1}r_{01}}{c} \quad (8b)$$

$$\omega_D = \frac{2\omega_{s1}v_{r1}}{c} \quad (8c)$$

and

$$u_{M2}(t) \propto \cos[\delta\omega t - \delta\varphi - \omega_{s1}\tau_a + \eta\sin(\omega_m(t-\tau_a)-\varphi_m)]$$
$$= J_0(\eta)\cos\Omega_1 - 2\sin\Omega_1 \sum_{n=0}^{\infty} J_{2n+1}(\eta)\sin[(2n+1)x_a] + 2\cos\Omega_1 \sum_{n=1}^{\infty} J_{2n}(\eta)\cos(2nx_a) \quad (9)$$

$$x_a = (\omega_m \pm \omega_{Dma})t - \frac{\omega_m(r_{01}+r_{02a})}{c} - \varphi_m \quad (10a)$$

$$\omega_{Dma} = \frac{\omega_m(v_{r1}-v_{r2a})}{c} \quad (10b)$$

$$\Omega_1 = (\delta\omega \pm \omega_{Da})t - \frac{\omega_{s1}(r_{01}+r_{02a})}{c} - \delta\varphi \quad (11a)$$

$$\omega_{Da} = \frac{\omega_{s1}(v_{r1}-v_{r2a})}{c}. \quad (11b)$$

The frequencies f_{Dm} and f_{Dma} are in the range of 10^{-2} Hz and, therefore, negligible. The principle spectra of the mixer signals in channels 1 and 2 are shown in Fig. 2. In module 1, the Doppler signal with frequency f_D is available in the baseband and symmetrically around the harmonic frequencies

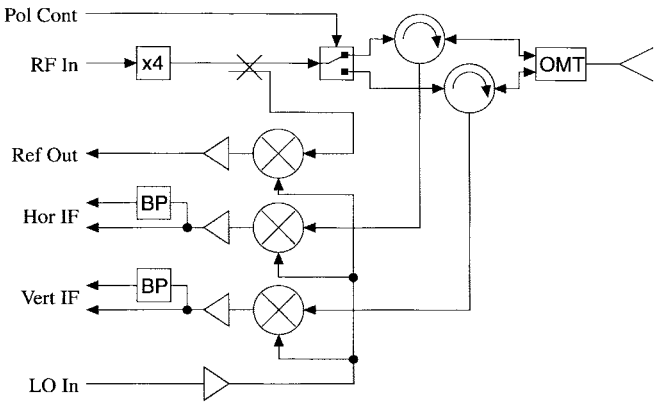

Fig. 8. Block diagram of the bistatic frontend.

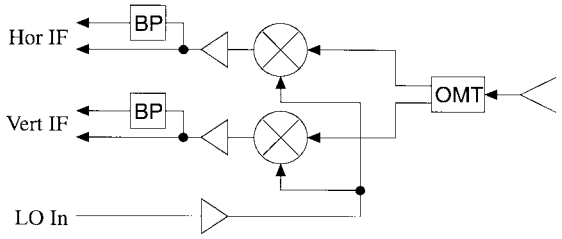

Fig. 9. Block diagram of the monostatic frontend.

of the modulation frequency. Two sidebands are located at the harmonics of the modulation frequency of the mixer signal of channel 2. From there, the Doppler difference frequency f_{Da} can be obtained. The distance to the ground r_{01} can be extracted from the Bessel spectra.

The parameters to be determined (ζ, h, v) are related to the measured values by

$$r_{01} = \frac{h}{\sin\vartheta} \quad (12a)$$

$$\vartheta = \vartheta_0 - \zeta \quad (12b)$$

$$f_D = \frac{2}{c} f_{s1} v\cos\vartheta \quad (13)$$

$$f_{Da} = \frac{1}{c} f_{s1} v(\cos\vartheta - \cos\gamma) \quad (14a)$$

$$\gamma = \gamma_a + \zeta, \quad (14b)$$

$$\gamma_a = \arctan\left(\frac{d\cos\zeta - h\,\mathrm{ctg}(\vartheta_0-\zeta)}{h + d\sin\zeta}\right) - \zeta. \quad (15)$$

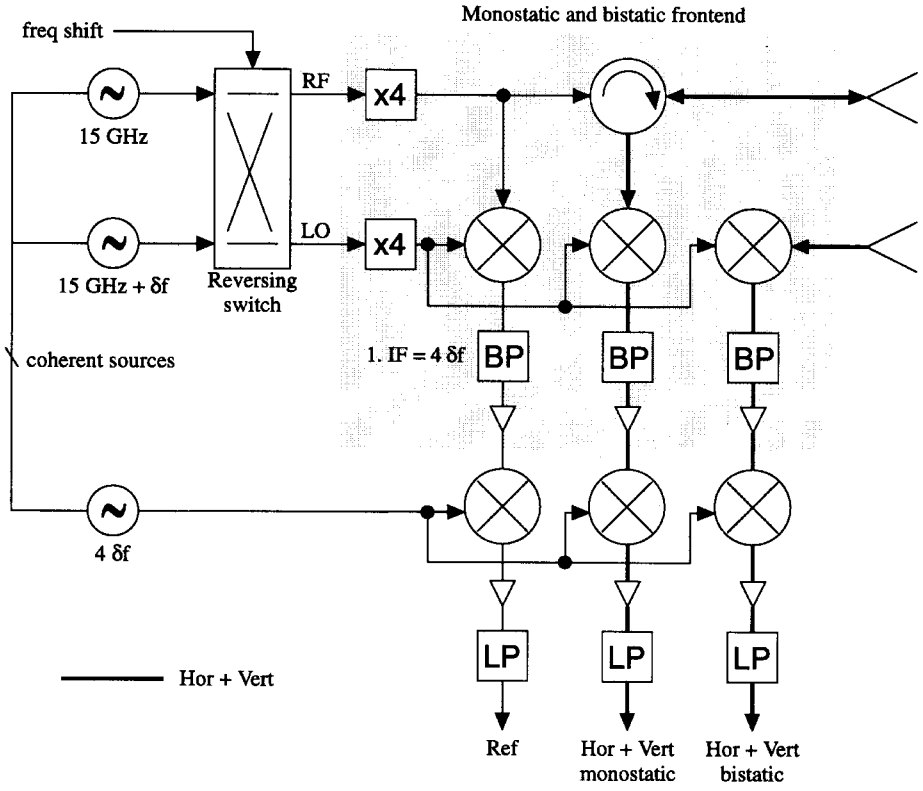

Fig. 10. 2F CW radar using two fixed tuned sources.

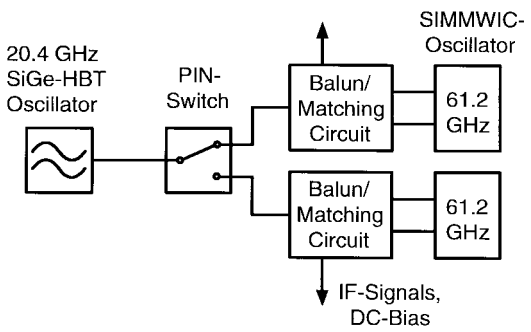

Fig. 11. Block diagram of the integrated radar frontend.

By solving (16)

$$F_\zeta = (1+AW)\cos(\vartheta_0-\zeta) - Q\cos\zeta = 0 \tag{16}$$

$$A = \sqrt{1+Q^2-2Q\cos\vartheta_0} \tag{17a}$$

$$W = 1 - \frac{2\omega_{Da}}{\omega_D} \tag{17b}$$

$$Q = \frac{d}{r_{01}} \tag{17c}$$

follows the tilt angle ζ. Examples for different W are given in Fig. 3.

The height above ground and the velocity can then be determined by

$$h = r_{01}\sin(\vartheta_0-\zeta) \tag{18}$$

$$v = \frac{c}{2}\,\frac{\omega_D}{\omega_{s1}}\,\frac{1}{\cos(\vartheta_0-\zeta)}. \tag{19}$$

III. Sensor Hardware

For automotive application, flat antennas are desired. Good accuracy in Doppler measurement demands high antenna gain. Both duties can be fulfilled by leaky-wave antennas. Fig. 4 shows the construction of leaky-wave antennas in principle.

The leaky-wave structure mainly consists of two dielectric layers—normally air and a dielectric slab over a metalized ground plane [2]. Excitation can be done, for example, in the conductive ground plane by a dipole or an open waveguide end. The excitation may be considered either as a horizontal electric dipole (HED) or a horizontal magnetic dipole (HMD). The feeding point determines the radiation angle, while gain can be adjusted by the dielectric constant of the slab.

For application in the sensor, a circularly shaped leaky-wave antenna with 20-dB gain and 00 radiation angle has been designed. The calculated antenna diagram is depicted in Fig. 5. Although leaky-wave antennas may provide oblique radiation angles, good cross polarization can only be achieved with radiation normal to the aperture. In order to find the cheapest possible way of manufacturing the sensor antennas, we have to investigate the influence of tolerances of the dimensions on the antenna gain.

Although deviations in the thickness of the air gap have more influence on the antenna gain, we look at the maximum allowed deviation of the parameters of the ceramic slab. The tolerances of the air layer are met by application of the injection moulding technique. The price of the substrate will grow very fast with decreasing tolerances.

In Figs. 6 and 7, we can see the maximum allowed deviation of thickness and permittivity to keep the gain deviation smaller

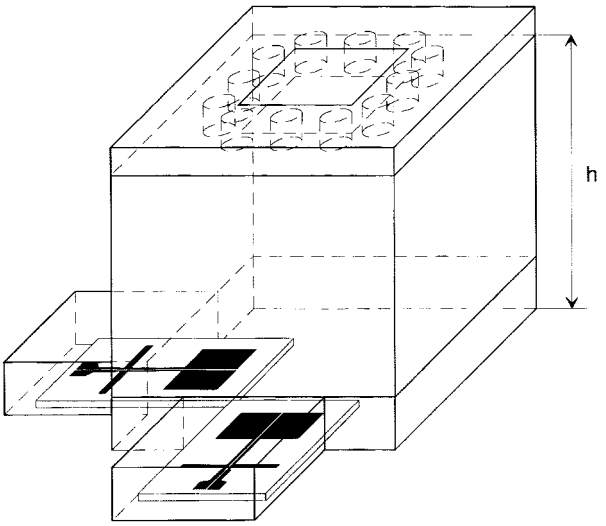

Fig. 12. Schematic view of the integrated SIMMWIC frontend.

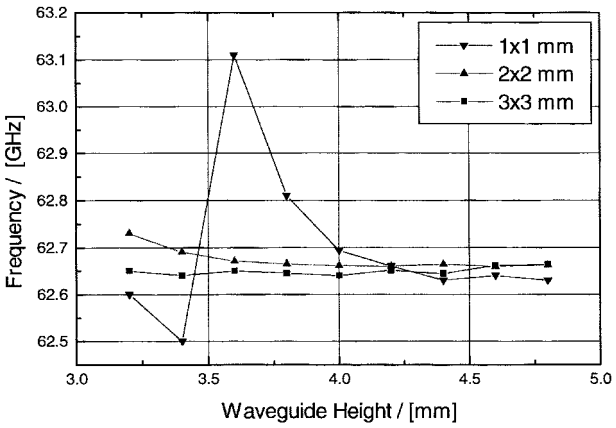

Fig. 13. Oscillating frequency of the integrated frontend over the height of the cavity. Parameter is the aperture of the iris.

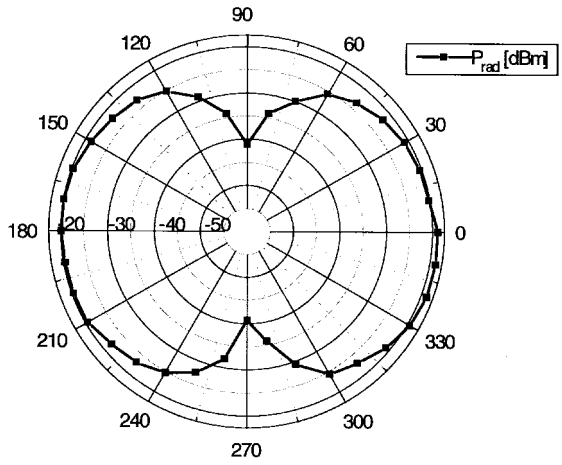

Fig. 14. Polarization pattern of the frontend.

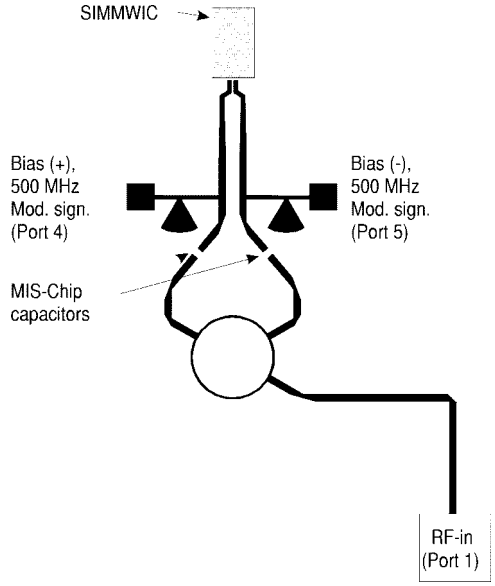

Fig. 15. Layout of the balun circuit.

than 3 dB. There are different graphs for HED and HMD excitation. Note that deviation in permittivity is rather uncritical, compared to deviation in thickness. It is also obvious that negative tolerances do not affect the antenna gain as much as positive tolerances. The reason is that in case of positive deviation, the antenna begins to squint. This means that the radiation pattern gets two major lobes at oblique angles with a very fast decreasing minimum in the 0° direction. As expected for a resonant structure, the sensitivity on tolerances grows with the permittivity of the dielectric substrate.

IV. Sensor Hardware

A. Waveguide Setup

In order to achieve measured data for an early development and optimization of the signal-processing algorithms, an experimental system in conventional hollow waveguide technique has been built up. It consists of two frontends which correspond to the two integrated frontends in the sensor concept and of data acquisition devices to process the IF signals. During the first measurements, a vector network analyzer (VNA) has been used. Later, a digital sampling unit will be applied.

The block diagrams of the two frontends are shown in Figs. 8 and 9. The monostatic frontend has the capability to synchronously send and receive, while the bistatic frontend is designed just to receive. In the monostatic frontend, the transmitted signal is generated by a frequency quadrupler. The downconversion of the received signals is done by harmonic mixers, which are pumped at the fourth subharmonic of the LO signal. In fact, the RF and LO reference signals are in the 15-GHz range. Thus, they can be guided by coaxial lines, which are easy to handle. A transistor–transistor logic (TTL) controlled single-pole double-throw (SPDT) switch makes it possible to alternately transmit horizontal (H) or vertical (V) polarization. The separation of the two polarizations is done by an orthomode transducer (OMT) for the transmitting and receiving case. Due to this, both frontends are suitable for full polarimetric operation. In general, the 15-GHz input RF signal may be frequency modulated. Therefore, the frontends are also suitable for the investigation of the sinusoidal frequency-modulation technique.

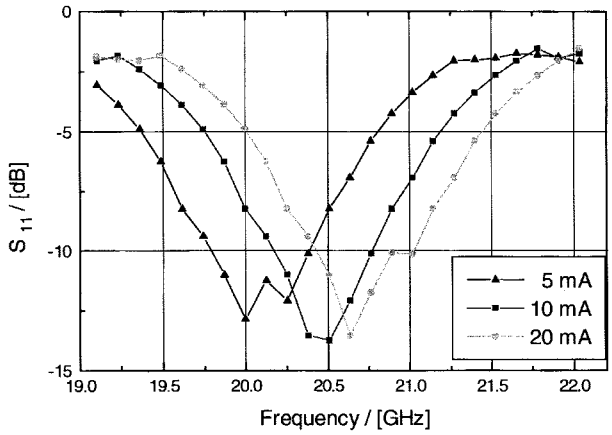

Fig. 16. Measured input return loss of the balun.

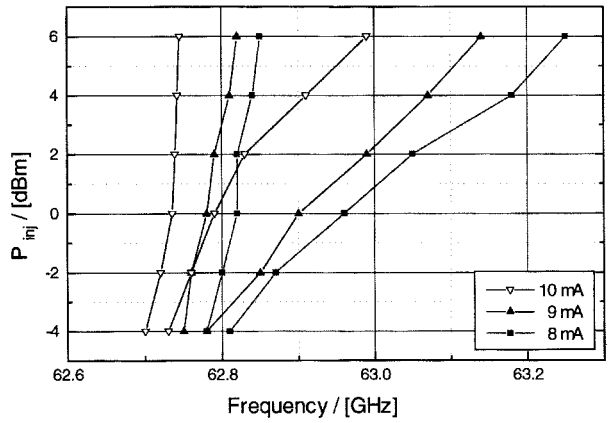

Fig. 17. Locking bandwidth of the SIMMWIC frontend.

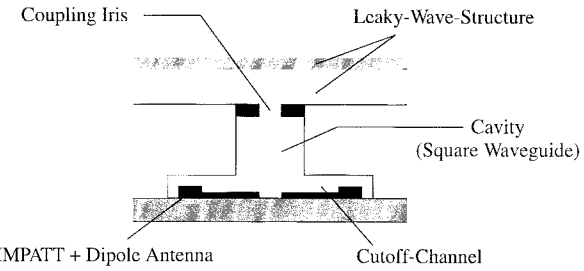

Fig. 18. Coupling structure (cross-sectional view).

The first experiments done with these frontends were polarimetric measurements. The polarimetric scattering parameters of several possible road surfaces like wet or dry asphalt and concrete have been measured. Therefore, the coherent RF and LO sources have been tuned to an IF of 20 MHz, which is required by the VNA. The probe was illuminated either with H or V polarization and the backscattered H and V components were simultaneously received with the two input channels of the VNA.

To achieve good accuracy in height measurement, the modulation frequency must be in the order of 50 MHz with a frequency deviation of 180 MHz. Because of the difficulties in generating this signal with common synthesizers, another modulation technique has been established for use in the experimental waveguide system. As there is only one major

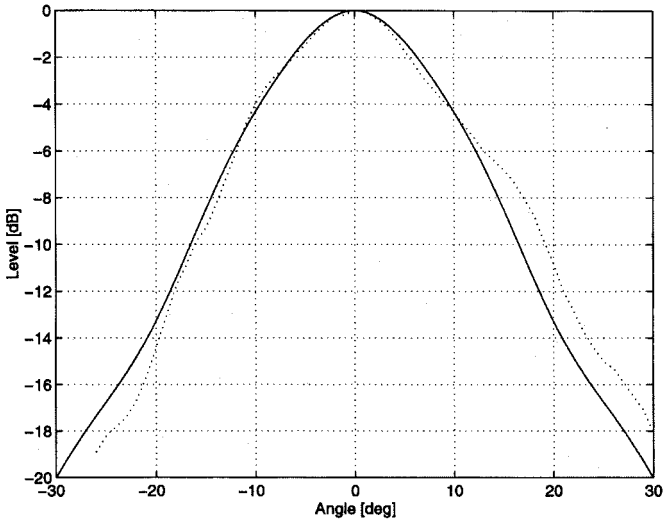

Fig. 19. Radiation pattern in E-plane.

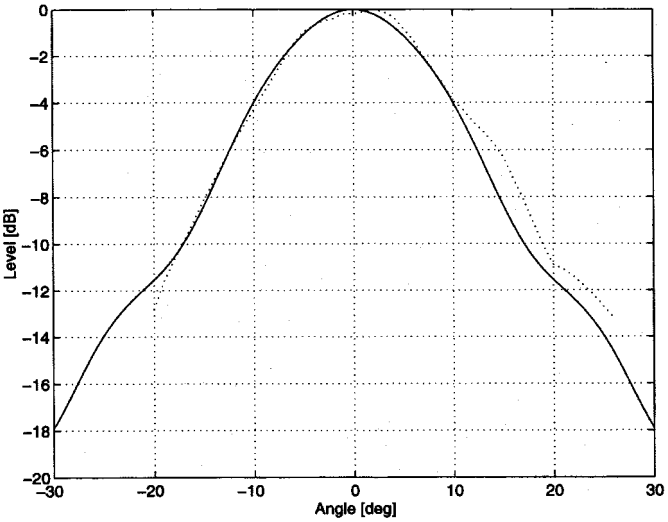

Fig. 20. Antenna diagram in H-plane.

target, namely the street surface, range measurements are also possible by transmitting only two frequencies, either simultaneously or alternately. This would allow one to use two fixed frequency sources which can be commutated by p-i-n switches. Using these two commutated signals as RF and LO leads to an IF, which is constant at four times the frequency difference. In this system, the IF is chosen to be 100 MHz. After amplification of the IF, another coherent 100-MHz source may convert this IF to zero before it is applied to the sampling unit. Fig. 10 shows this concept.

B. Integrated Frontend

A block diagram of the integrated frontend is depicted in Fig. 11. Monolithically integrated SIMMWIC oscillators [3] generate the transmit signal. Each chip transmits one linearly polarized wave. Two SIMMWIC transmitters are, therefore, necessary to support the polarimetric mode of the radar. The detection of the backscattered signals is accomplished by application of the self-mixing properties of the millimeter-wave oscillators [4]. Frequency stabilization of the frontend

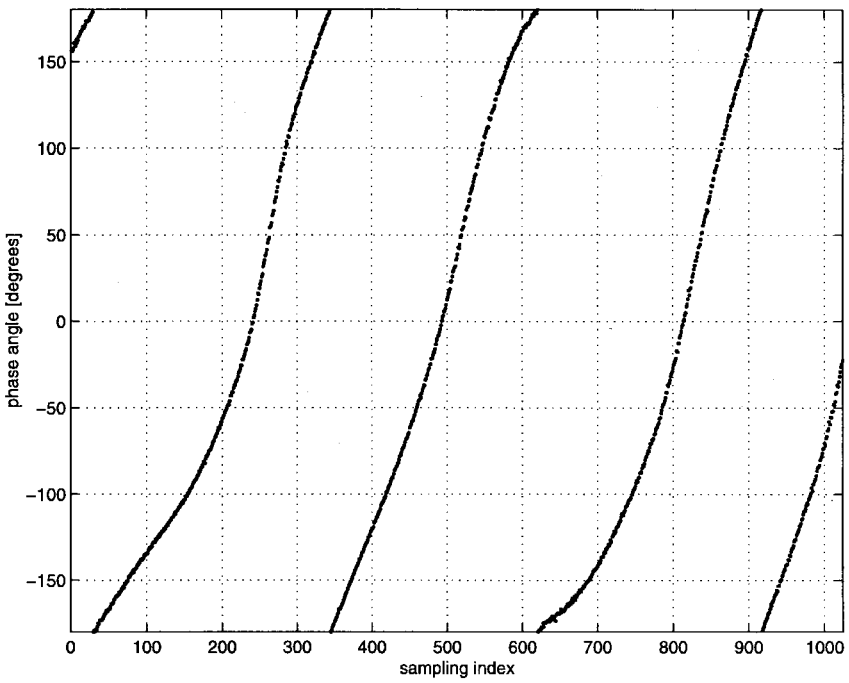

Fig. 21. Phase of S_{hh} caused by Doppler effect.

is realized by subharmonic injection locking [5], [6] of the frontend at the third subharmonic. Therefore, the integrated frontend is fed with a reference signal at a frequency of 20.4 GHz.

It is inevitable for the operation of a radar system in automotive applications to hermetically shield the millimeter-wave circuits from environmental factors like dust, water spray, and corrosive atmosphere. A new topology was, therefore, investigated for the mounting of the millimeter-wave circuits. Both SIMMWIC's are located in sections of waveguide which are operated below cutoff. The radiating structure is coupled to a waveguide section with square cross section. This cavity itself is coupled to a planar leaky-wave antenna by an iris. To hermetically seal the structure, the iris is realized by a slab of ceramic, which is metallized on both sides. Both metallizations are shorted by metallized via holes at the edges of the iris to prevent the excitation of parallel plate modes. The waveguide section consists of a metallized powder injection moulding (PIM) part. The bottom of the waveguide is closed by a multilayer low-temperature cofired ceramic (LTCC) substrate on which the millimeter-wave circuits are mounted. This substrate also provides a feedthrough for dc and RF signals below the walls of the PIM structure in a deeper wiring layer. The three parts of the frontend housing are assembled by solder techniques. A schematic view of the integrated frontend is shown in Fig. 12.

An experimental investigation of the integrated frontend has been carried out by a model which has been milled in brass, thus being able to investigate the influence of the height h of the waveguide section and the shape of the iris on the transmitted power and frequency of the frontend. Fig. 13 shows the oscillating frequency of the integrated frontend over the height of the cavity. The width of the square iris has been chosen as a parameter. As can be seen, there is only little effect of the waveguide height on the oscillating frequency for large apertures of the iris, which means that assembly tolerances are not critical. Significant pulling of the frequency is observed only in the case of the narrowest iris.

Fig. 14 is a plot of the power which is received if the transmitter frontend is rotated with respect to the z-axis. The cross polarization is better than 20 dB. Even though the topology of the frontend is not strictly symmetric with respect to the x- and y-axes, the E-plane of the transmitted wave is not tilted.

As mentioned above, the frontend is tied to a reference by subharmonic injection locking. The active element is inserted between the two conductors of a two-conductor coplanar stripline. The transition from microstrip to coplanar line, along which only the odd mode is excited, is realized by a rat-race coupler. The layout of the balun is depicted in Fig. 15. Low-pass filters are added for biasing the diode and extraction of the IF signals. MIM capacitors are necessary to prevent a dc short circuit by the rat-race coupler.

The planar circuit has been modeled by use of the commercially available design tool HP MDS. The measured input return loss of the frontend at the third subharmonic is depicted in Fig. 16. The parameter is the dc current through the active device. An input return loss of below -10 dB is achieved over a bandwidth of more than 500 MHz.

The system specifications demand a locking bandwidth which is wide enough to cover the full available bandwidth of 350 MHz. Fig. 17 shows that locking bandwidths of up to 400 MHz are realized at a moderate locking power.

For the application in a compact sensor device, the integrated frontend has to be coupled to the leaky-wave structure, such that the complete construction remains flat. The leaky-wave antenna is fed by a square waveguide. This makes the symmetrical excitation of both polarizations possible.

A centered coupling iris with square cross section should provide impedance matching between the waveguide and the antenna without seriously affecting cross polarization. The two orthogonal modes of the feeding waveguide are excited by two pairs of IMPATT oscillators realized in SIMMWIC technology. Fig. 18 shows the coupling structure in principle. It may be realized as a metallized plastic-molded piece.

In this way, the square waveguide acts as a resonant cavity to increase the external Q of the oscillators. The side channels in which the oscillators are mounted have dimensions below cutoff. For that reason, they are not expected to affect the cavity properties. The coupling iris must also provide hermetical sealing. Therefore, it will be manufactured as a metallized ceramic plate with through connections around the edge of the iris.

V. Measurement Results

The coupling structure shown in Fig. 18 has been realized as a milled part. It consists of the cutoff channel structure with the cavity and a square-shaped leaky-wave antenna with a dimension of 40 mm $\times$ 40 mm. In Figs. 19 and 20, the measured (dotted) and calculated (solid) radiation patterns of this active antenna are shown.

For first testing the frontends performance, the polarimetric scattering parameters of slowly moved samples from road surfaces have been measured in the laboratory. In Fig. 21, the phase of the scattering parameter S_{hh}, which contains the Doppler information about the velocity, is depicted.

VI. Conclusions/Outlook

The concept of a multifunctional radar sensor for automotive applications has been treated in this paper. A waveguide setup is realized to proof the functionality of the system and to collect measurement data in an early stage of development. The integration of SIMMWIC's in an integrated frontend, which is suitable for mass volume production, is presented. The total height of the frontend is reduced by the application of a planar antenna, which reduces the dimensions of the sensor dramatically. The proposed geometry is well suited for application in the integrated frontend of the system. Its key features are the reduction of the operating current of the millimeter-wave chips and the excellent polarization purity of the transmitted signals, which is essential for polarimetric measurements. Further work will deal with the proper design of the integrated frontend, even though the specifications are fulfilled.

References

[1] H. H. Meinel, "Commercial applications of millimeter waves: History, present status and future trends," *IEEE Trans. Microwave Theory Tech.*, vol. 43, pp. 1639–1653, July 1995.

[2] H. Ostner, E. Schmidhammer, J. Detlefsen, and D. R. Jackson, "Radiation from dielectric leaky-wave antennas with circular and rectangular apertures," *Electromagnetics*, vol. 17, no. 5. pp. 505–535, Sept./Oct. 1997.

[3] J.-F. Luy, K. M. Strohm, H.-E. Sasse, A. Schueppen, J. Buechler, M. Wollitzer, A. Gruhle, F. Schaeffler, U. Guettich, and A. Klaaßen, "Si/SiGe MMIC's," *IEEE Trans. Microwave Theory Tech.*, vol. 43, pp. 705–714, Apr. 1995.

[4] M. Claassen and U. Guettich, "Conversion matrix of self-oscillating mixers," *IEEE Trans. Microwave Theory Tech.*, vol. 39, pp. 25–30, 1991.

[5] M. Wollitzer, J. Buechler, and J.-F. Luy, "Subharmonic injection locking (of) slot oscillators," *Electron. Lett.*, vol. 29, no. 22, pp. 1958–1959, 1993.

[6] M. Singer, K. M. Strohm, J.-F. Luy, and E. M. Biebl, "Active SIMMWIC-antenna for automotive applications," in *IEEE-MTT-S Conf. Dig.*, Denver, CO, June 8–13, 1997, pp. 1265–1268.

Michael Wollitzer was born in Landsberg, Germany, in 1967. He received the Dipl. Ing. degree in electrical engineering from the Technische Universität München, München, Germany, in 1993.

Since 1993, he has worked as a Research Assistant at the Daimler-Benz Research Center, Ulm, Germany, where he is engaged in the development of silicon-based solid-state devices and planar millimeter-wave circuits. His interests also include the investigation of near-range radar sensors and their realization by application of planar integration techniques.

J. Buechler, for photograph and biography, see this issue, p. 676.

J.-F. Luy (M'86–SM'95), for photograph and biography, see this issue, p. 570.

Uwe Siart was born in Bayreuth, Germany, on March 16, 1969. He received the Dipl.-Ing. degree in electrical engineering from the Friedrich-Alexander-Universität Erlangen-Nürnberg, Nürnberg, Germany, in 1996.

Since 1996, he has been a Research Assistant at the Lehrstuhl für Hochfrequenztechnik, Technische Universität München, München, Germany, where he is involved with the design of a multifunctional near-range radar sensor. His research interests include appropriate signal-processing techniques in the interaction between the various modulation techniques and special hardware concepts, and in near-range scattering from rough surfaces.

E. Schmidhammer, photograph and biography not available at the time of publication.

J. Detlefsen (M'82), photograph and biography not available at the time of publication.

M. Esslinger, photograph and biography not available at the time of publication.